Hindawi
Advances in Civil Engineering
Volume 2022, Article ID 5365789, 15 pages
https://doi.org/10.1155/2022/5365789

Research Article

Carbonation Characteristics and Bearing Capacity Attenuation of Loaded RC Beam Coupled with Chloride Erosion

Xiangong Zhou,[1] **Xiaoyu Zhang**,[1,2] **Gang Li**,[3] **and Jialu Li**[1]

[1]*School of Highway, Chang'an University, Xi'an 710064, China*
[2]*China Railway First Survey and Design Institute Group Co., Ltd., Xi'an 710043, China*
[3]*Shaanxi Transportation Holding Group Co., Ltd., Xi'an 710065, Shaanxi, China*

Correspondence should be addressed to Xiangong Zhou; zhouxiangong@163.com

Received 3 March 2022; Accepted 18 June 2022; Published 15 July 2022

Academic Editor: Bang Yeon Lee

The durability of a concrete bridge structure is a systematic problem composed of material, structure, natural environment, and service environment. Various factors are coupled, which affect each other, and single-factor research cannot fundamentally solve this problem. In this paper, the carbonation characteristics of RC beams with different loading states under the coupling action of carbonation and chloride erosion are studied. Through the experiment, the author tries to find the influence of stress state and chloride ion erosion on the carbonation of concrete and analyze the failure mode and the attenuation rules of the flexural and shearing capacity of the corroded RC beams under the coupling action. For this purpose, five groups of experiments under different working conditions were designed, including chloride ion erosion and carbonation experiments without external load of the cubic blocks, and chloride erosion and carbonation coupling experiments of RC beams under different stress states and stress levels. The carbonation rate of concrete can be reduced by 56%~60% under the coupling action of chloride salt. Different loading states and stress levels have an obvious influence on carbonation and chloride ion corrosion, which further affects the corrosion rate of steel bars. Under a low corrosion rate, the bending and shear failure modes of the corroded beams are similar to those of the noncorroded beams, and the section strain distribution still approximately conforms to the plane section assumption. The relationship between the relative ultimate shear strength or the relative ultimate flexural strength and the average section-corrosion rate of the reinforcement is approximately linear.

1. Introduction

Concrete carbonation will make the reinforcement lose its alkaline protection, cause corrosion and volume expansion of the reinforcement, and thus crack the concrete cover and reduce the effective cross-section area of the reinforcement, which seriously affects the durability and service life of the concrete bridge structures [1–3]. However, in May 2020, sensors at NOAA's Monaloa Observatory detected an alarming data that the atmospheric carbon dioxide measured reached a seasonal peak of 417.1 parts per million, the highest monthly reading ever recorded [4], and it was expected to rise to 650 ppm by 2100 [5]. There is no doubt that the increase of CO_2 concentration in the atmosphere will aggravate the carbonation of concrete. Therefore, it is of great practical significance to study the carbonation of concrete structures, especially of lifeline projects, such as bridges.

In the 1980s~1990s, Papadakis [1, 6–9] constructed a prediction model for carbonation depth based on the carbonation mechanism and Fick's diffusion law. Since then, large numbers of scholars have modified the carbonation model on this basis. Some scholars take the water-cement ratio as the main parameter to experiment [10, 11], while some scholars take the water-cement ratio and cement content as research objects [12–14]. Niu et al. obtained the relationship between concrete compressive strength and carbonation depth through regression analysis, according to a large amount of experimental data [15]. Some scholars have studied the relationship between load and concrete carbonation through experiments. Wang et al. obtained the

carbonation coefficient of concrete subjected to different levels of nondestructive axial tensile and compressive loads [16]. Jiang et al. took the residual strain of concrete in a compression state as the damage index and established the CO_2 diffusion coefficient, including the residual strain [17].

From the perspective of research methods, these pieces of research can be divided into theoretical models based on the carbonation mechanism and empirical models based on test results, and these pieces of research combined the two. In terms of the property of the models, these models can be divided into three types, which are as follows: the deterministic model [6–17], stochastic model [18], and other models based on the neural network, grey system theory, cellular automata, and other theories [19, 20]. From the perspective of research objects, most of these pieces of research are based on the material, while a few are based on the component or structure. As we know, carbonation, freeze-thaw, chloride, and sulfate are the major factors affecting the durability of concrete, however, most of these pieces of research consider only one of them, and only a few scholars consider the interaction of these factors. For example, some scholars have studied the influence of carbonation on chloride ion corrosion, however, the research on the influence of chloride ion on carbonation is rarely mentioned [21, 22]. Some scholars have studied the effect of load on carbonation, however, a few people have mentioned the effect of load on carbonation under the coupled action of chloride ion erosion [23, 24]. Wang et al. reported the influence of structural loading on the carbonation of three types of concrete, namely Portland cement (PC), PC with 30% of FA, and PC with 50% of GGBS, and presented the evaluation of the carbonation coefficients [23]. Miao et al. performed fast carbonization tests for concrete with respect to the fatigue damage and established a durability prediction model for concrete under the combined action of carbonization and fatigue loading of vehicles [24].

Nevertheless, the durability of concrete is a systematic problem composed of material, structure, natural environment, and service environment, and so is the study of the carbonation of concrete bridges. The bridge structure is usually corroded by many complex media at the same time. The study of the durability of the bridge structure must focus on the actual service environment and applied load characteristics. That is to say, the coupling effect of various erosion factors should be considered, however, limited research has been carried out in this area [25, 26].

In addition, for the concrete bridge structure corroded by many factors, the engineers not only need to know its carbonation performance to determine the thickness of the protective layer in the design but also need to know the deterioration of the structure caused by corrosion to predict and evaluate the bearing capacity and remaining life of the existing structure. Tian et al. investigated the combined effects of corrosion rate, concrete cover thickness, and stirrup spacing on the bond performance between the reinforcement and the concrete of reinforced concrete (RC) specimens through a pullout test [27]. Torres-Acosta et al. conducted an experimental investigation on the flexure capacity loss of RC beams with corroded reinforcement. The research results indicated that the flexure capacity decreased mainly because of the formation of pits on the reinforcement surface [28–30]. Campione and Cannella proposed a simple mechanical model to predict the load-deflection response of the RC beam in flexure and shear subjected to corrosion process, considering such main phenomena as the reduction of steel area, concrete strength reduction, bond degradation, and reduction in the working stress of stirrups [31].

Because of such complex material properties of concrete as a multiphase, porous, and multicomponent, and the complexity of the service environment and the applied load of the concrete bridge structure, there are many complex factors affecting carbonation. These factors are coupled with each other, resulting in many prediction methods. Nevertheless, there are still some problems puzzling the researchers that need to be resolved, which are as follows:

(1) Chloride erosion and carbonation often occur at the same time in the concrete bridge structure. Some scholars have studied the influence of carbonation on chloride transport, however, the influence of chloride erosion on carbonation is rarely discussed. The influence of chloride erosion on carbonation needs to be further studied.

(2) The influence mechanism and the law of load on carbonation have been basically studied, however, the bridge structure itself is in a complex state of stress. Under the combined action of load-chloride ion erosion-carbonation, carbonation will inevitably show different characteristics, however, this research is rarely mentioned.

(3) Many bridge structures are prestressed concrete structures. Hence, the durability research of the prestressed concrete structure is particularly important. Some scholars use the axial compression state to replace the prestressed state when they study the carbonation of the prestressed concrete structure [32]. Whether this substitution relationship is reasonable needs further verification.

In view of the above problems, the authors designed five groups of experiments under different working conditions, including chloride ion erosion and carbonation experiments without the external load of the cubic block, along with chloride ion erosion and carbonation coupling experiments of RC beams under different stress states and stress levels. Then, the carbonation depths with time were measured in each group of the experiments. After these erosion tests, the ultimate bearing capacity tests of the corroded RC beams were carried out to investigate the influence of erosion on flexural and shear capacities. The flexural and shearing characteristics of the corroded beams were investigated, including failure mode, crack distribution, and load displacement/strain characteristics.

2. Experimental Program

The experiment program was developed into two parts: corrosion test and load test. The corrosion test was

conducted to measure the evolution of the carbonation depth with the coupling effect of carbonation/chloride corrosion and different stress states. The aim of the load test was to analyze the bearing capacity of specimens after the corrosion test.

2.1. Materials and Specimen Preparation. A total of five test groups, SP1~SP5, were carried out in this experiment. Specimen numbers and the types of tests they underwent are shown in Table 1. For each test group, two strength grades of the concrete were designed, C40 and C50, respectively. The mix proportion and compressive/tensile strengths of concrete are listed in Table 2.

For beams in group SP3~SP5, the section size is 100 mm × 150 mm, and the depth of concrete cover is 30 mm. The bottom of the beam is configured with two diameters of the 10 mm HPB 235 longitudinal rebars. The top of the beam is configured with two diameters of the 6 mm HPB 235 longitudinal rebars. The stirrup is the HPB 235 rebar of 6 mm diameter. The yield point and the tensile strength of the bar shall not be lower than 235 MPa and 370 MPa, respectively, and the elastic modulus is 2.1×10^5 MPa. The diagrams of geometric parameters and rebar parameters of the beams are shown in Figure 1.

All specimens were kept in the standard curing room for 28 days before the corrosion test or load test.

2.2. Corrosion Test. To simulate the natural climate environment of carbonation and chloride corrosion, the corrosion acceleration test was simulated, as shown in Figure 2, in an artificial climate chamber located in the structural climate environment laboratory. It can realize automatic temperature control and humidity control.

Referring to the carbonation acceleration method in the "Standard for test methods of long-term performance and durability of ordinary concrete" (GB/T50082-2009), the total duration of carbonation and salt-fog tests were determined as 28 days and 60 days, respectively. In particular, for specimens in group SP1, only the carbonation test was conducted and continued for 28 days. For specimens in groups SP2~SP5, the salt-fog test (15 days in one cycle) alternated with the carbonation test (7 days in one cycle), and a total of 4 cycles (88 days) were performed.

In the salt-fog test, the specimens were sprayed with 5% NaCl solution, and the temperature was kept at (20 ± 2)°C, with the relative humidity (RH) within (90 ± 5)% throughout the test. In the carbonation test, the specimens were carbonated with the following experimental conditions: (20 ± 2)°C, (70 ± 5)% RH, and (20 ± 3)% CO_2.

The four lateral surfaces of all specimens in corrosion tests were sealed by paraffin, leaving open the bottom and top surfaces, guaranteeing that CO_2/chloride diffuses into the concrete in one dimension. For all test groups, the carbonation depths of specimens were measured when the cumulative carbonation time reached 3, 7, 14, and 28 days, respectively, while the cumulative time of the corrosion test reached 18, 22, 44, and 88 days for specimens in groups SP2~SP5.

For each cubic specimen in groups SP1 and SP2, there existed 12 sample blocks. Every 3 sample blocks were taken out each measuring time. As shown in Figures 3(a) and 3(b), after cleaning the splitting surfaces of the sample blocks, a phenolphthalein pH indicator was sprayed over the surface. About 30 seconds later, the measuring instrument was used to inspect the carbonation depth, and a total of 8 measuring points were chosen on each cross-section. The average carbonation depth of 3 measuring sample blocks was used as the carbonation depth of specimens for analysis.

For each beam specimen in groups SP3~SP5, there existed two samples. Particularly for specimens in groups SP4 and SP5, one sample beam was used to measure the carbonation depth, whereas the other one was used to conduct the load test after corrosion. Because of the existence of rebars, it was difficult to split them like the cubic blocks. Therefore, the carbonation depth was measured by drilling holes on the concrete surface locally and then spraying the phenolphthalein pH indicator, as shown in Figure 3(c). Three locations in one sample beam were drilled each measuring time. Besides, to avoid the influence of crack/damage for further corrosion tests, the damaged areas were sealed with paraffin after each measurement. When finishing the whole carbonation process, the beams could be broken to obtain the final carbonation depth, which can be seen in Figure 3(d).

Before conducting the carbonation test, the initial carbonation depth should be tested. As shown in Figure 3(e), there was no carbonated area in the sample blocks. Therefore, it was considered that the initial carbonation depth was 0 mm.

To simulate the corrosion of beams under sustained stress in groups SP3~SP5, a special force-holding device was designed, as shown in Figure 4. The holding device consists of screw rods, screw caps, and a compression spring. A spring was covered on one end of the pull rods.

For specimens in group SP3 with the stress state of axial compression, the axial force was applied (Figure 4(a)). For specimens in group SP4 under pure bending, a holding device was used to apply the bending moment (Figure 4(b)). For specimens in group SP5 with a complex stress state of compression-bending, two holding devices were used simultaneously to apply compression and bending moment (Figure 4(c)).

By turning the screw cap, it can adjust the force on the spring to apply different load levels on the beam. The force value was determined according to the stress value at beam bottom, and the setting of stress values is listed in Table 1.

2.3. Load Test. After the corrosion test, the corroded beam specimens without damage were used to conduct the bending test (group SP4) and the shear resistance test (group SP5), as shown in Figure 5. The lifting jack was used to apply the loads, and the load values were controlled by the pressure sensor. To measure the strains at the midspan cross-section, strain gauges were set on the surface of the concrete. Dial indicators were set at both supports and the midspan position to measure the deflection of the beams.

Table 1: Specimens and test arrangement.

Group number	Specimen number		Specimen size (mm)	Corrosion test				Load test
	C40	C50		Carbonation	Chloride corrosion	Stress state	Stress at beam bottom (MPa)	
SP1	SP1-40	SP1-50	150 × 150 × 150	Yes	—	—	—	—
SP2	SP2-40	SP2-50	150 × 150 × 150	Yes	Yes	—	—	—
SP3	SP3-1-40	SP3-1-50	100 × 150 × 750	Yes	Yes	Axial compression	$0.3f_c$	—
	SP3-2-40	SP3-2-50					$0.5f_c$	
	SP3-3-40	SP3-3-50					$0.7f_c$	
SP4	SP4-0-40	SP4-0-50	100 × 150 × 1500	—	—	—	—	Bending test
	SP4-1-40	SP4-1-50		Yes	Yes	Pure bending	0	
	SP4-2-40	SP4-2-50					$0.3f_t$	
	SP4-3-40	SP4-3-50					$0.5f_t$	
SP5	SP5-0-40	SP5-0-50	100 × 150 × 750	—	—	—	—	Shear test
	SP5-1-40	SP5-1-50		Yes	Yes	Compression-bending	0	
	SP5-2-40	SP5-2-50					$0.15f_c$	
	SP5-3-40	SP5-3-50					$0.3f_c$	

Table 2: Mix proportion of concrete and compressive/tensile strength.

Concrete grade	Cement (kg/m^3)	Water (kg/m^3)	Sand (kg/m^3)	Crushed stone (kg/m^3)	Admixture (kg/m^3)	Compressive strength f_c (MPa)	Tensile strength f_t (MPa)
C40	426	162	763	1014	8.5	43.05	1.20
C50	490	162	594	1206	8.8	54.04	1.32

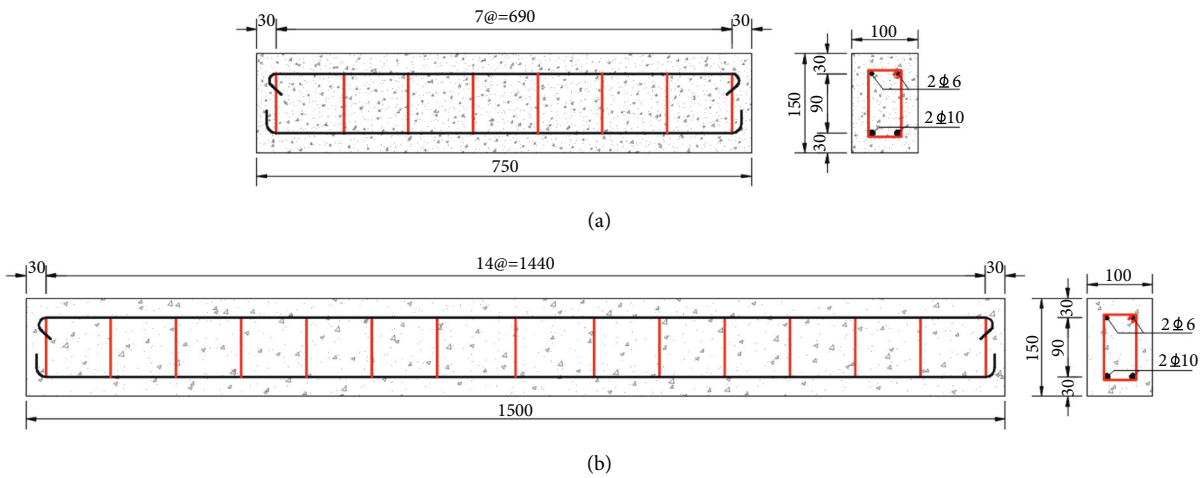

Figure 1: The arrangement of stirrups and longitudinal reinforcement of specimens. (a) Specimens in groups SP3 and SP5. (b) Specimens in group SP4 (unit: cm).

3. Analysis on Carbonation Characteristics

3.1. Effect of Chloride Corrosion. Figure 6(a) shows the carbonation depth of specimens in groups SP1 and SP2 during the corrosion test. It can be found that the carbonation depths of specimens in SP1 without chloride corrosion are significantly higher than those in SP2 with chloride ion erosion. That is to say, chloride corrosion inhibits the carbonation of concrete, and the carbonation rate is greatly reduced.

Actually, this phenomenon can be explained by two aspects of chemical and physical effects [33]. From a physical standpoint, the chloride ions will precipitate in the form of solid particles during the evaporation of water in the pore solution. Hence, the pore structure is compact, and the total porosity factor is lowered. The diffusion rate of CO_2 will slow down, and the carbonization of the cubic block is inhibited to some extent. From the chemical viewpoint, the chloride ion will form a chemical adsorption layer on the surface of the CSH gel, which also reduces the porosity and decreases the carbonization rate. According to the test data and the corresponding environmental conditions, it is calculated that chloride corrosion can reduce the carbonation rate of concrete by 56%~60%.

(a) (b)

Figure 2: Laboratory of structural climate environment. (a) External appearance. (b) Internal arrangement.

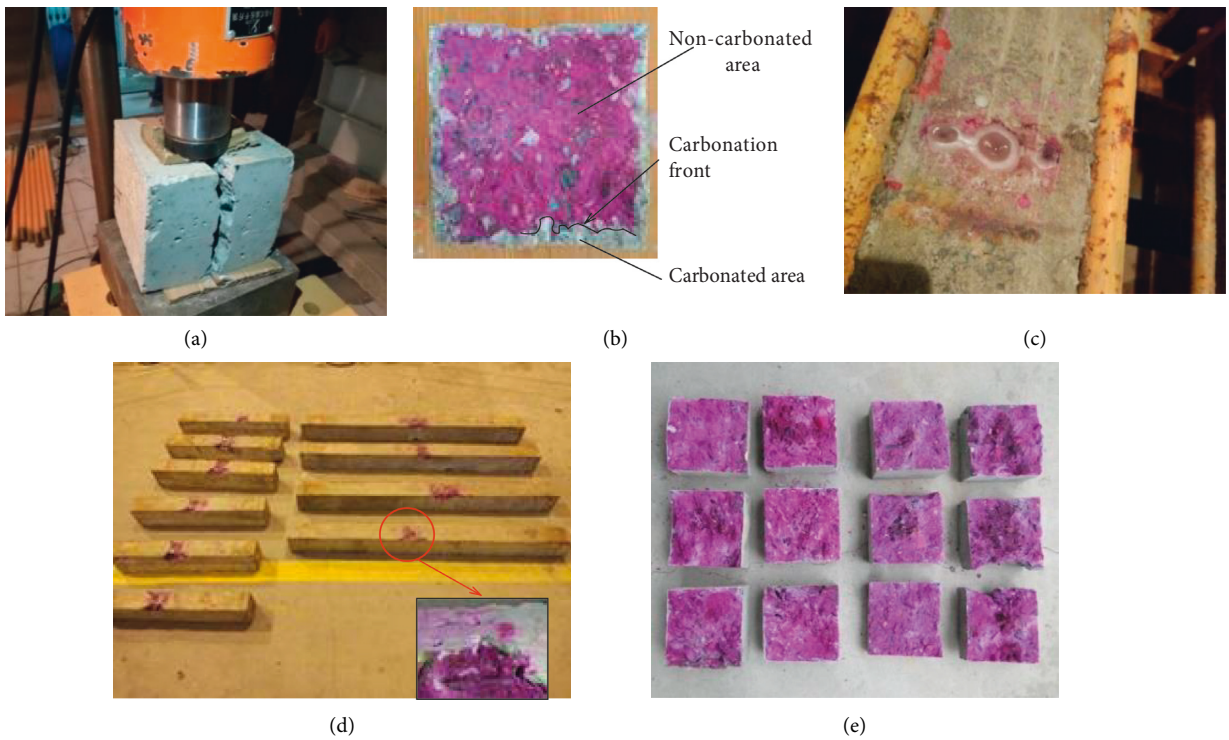

(a) (b) (c)

(d) (e)

Figure 3: Carbonation depth measurement of specimens. (a) The cube cleavage test of specimens in groups SP1 and SP2. (b) One splitting surface of sample blocks with phenolphthalein. (c) The measurement of carbonation depth of beams in groups SP3~SP5 during the corrosion test. (d) The measurement of the carbonation depth of beams in groups SP3~SP5 after the carbonation test. (e) The degree of carbonation depth before the carbonation test.

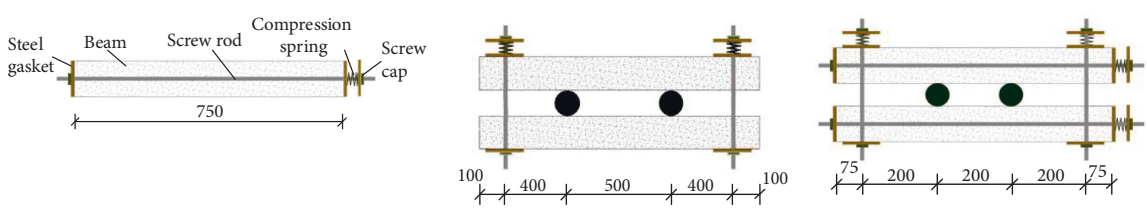

(a) (b) (c)

Figure 4: Force-holding devices and specimens. (a) Holding device in SP3 to apply axial force. (b) Holding device in SP4 to apply bending moment. (c) Holding device in SP5 to apply compression and bending moment (unit: mm).

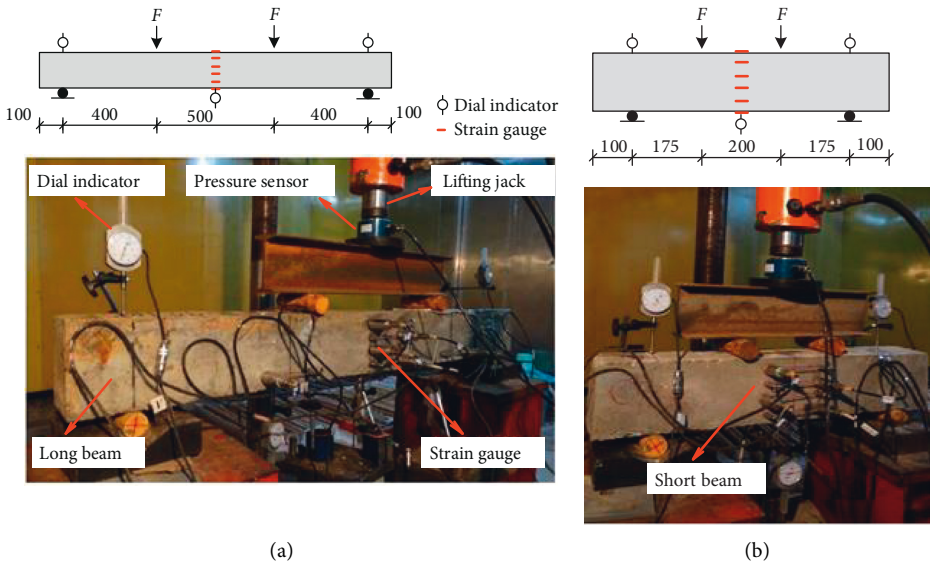

Figure 5: Measuring devices and loading system of load tests. (a) Bending test for specimens in group SP4. (b) Shear test for specimens in group SP5.

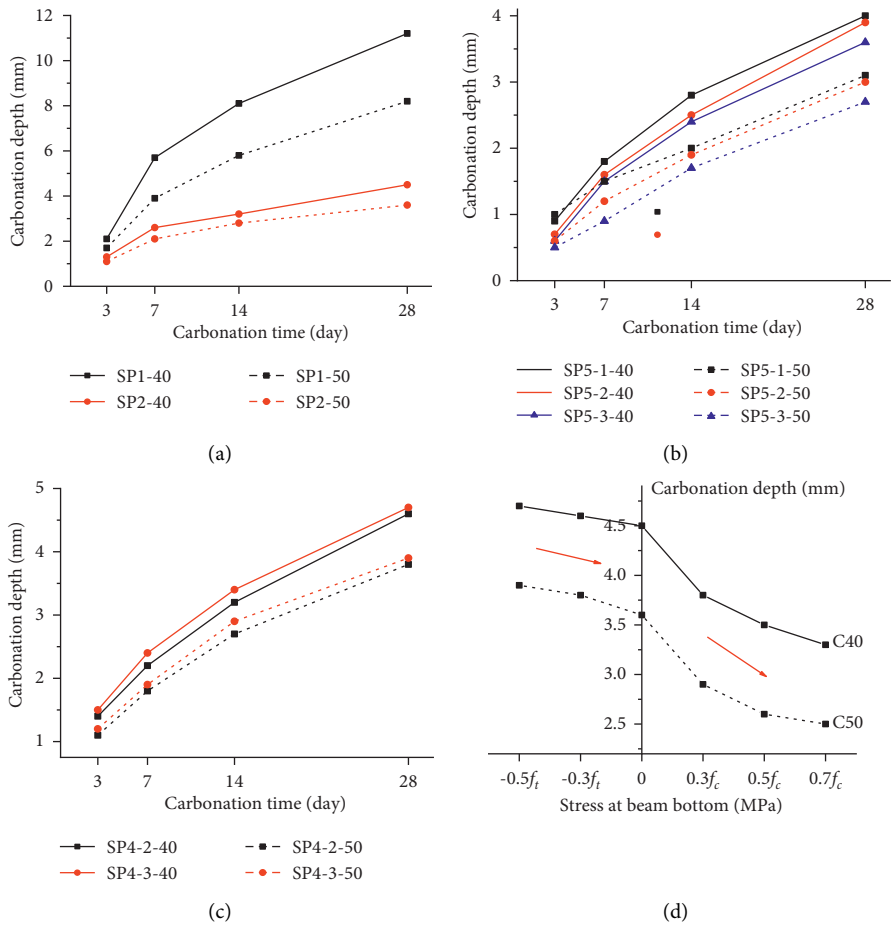

Figure 6: The results of carbonation depths during the corrosion test. (a) Specimens in groups SP1 and SP2. (b) Specimens in group SP5. (c) Specimens in group SP4. (d) Carbonation depth at 28 days.

3.2. Effect of Stress State. The carbonation depths of specimens in group SP5 are shown in Figure 6(b). It can be seen from the figure that the variation trend of the carbonation depth with time is similar to that in cubic specimens, however, the depth value has much difference. For the same concrete grade, the carbonation depth decreases with the increase of compressive stress level, indicating that the compressive stress restrains the carbonation rate.

The carbonation depth of beams in SP4 is drawn in Figure 6(c). Compared with the results of the compressive state at the same carbonation time in Figure 6(b), the carbonation depths of beams in the tensile stress are larger, and they are also larger than those without an external load in group SP2 in Figure 6(a), which indicates that the tensile stress tends to accelerate the carbonation rate.

Generally, the test data reflects that the stress state of beams will have a significant effect on the carbonation rate of concrete. Specifically, the compressive stress will reduce the carbonation rate, while the tensile stress will promote the carbonation rate. To show this effect more clearly, the carbonation depths of specimens with different concrete grades in groups SP3 and SP4 on the 28^{th} day of carbonation are depicted in Figure 6(d). It can be seen that with the decrease of tensile stress and then the gradual increase of the compressive stress, the carbonation depth decreases successively for both concrete grades of C40 and C50. This phenomenon can be explained by the fact that the applied stress can cause a change in the pore structure and porosity and then lead to a change in the carbonization rate. The compressive stress will reduce the porosity, thus reducing the carbonation rate, while the effect of tensile stress is the opposite. However, because of the fact that the tensile strength of concrete is far lower than its compressive strength, the impact of compressive stress on porosity and carbonation rate is more remarkable than that of tensile stress in the same percentage of increase or decrease of stress value. Therefore, as reflected in Figure 6(d), the curves of carbonation depth become steeper under a compressive state.

3.3. Discussion on Axial and Eccentric Compression. As discussed above, the increase of compressive stress will reduce the porosity of the concrete and the carbonation rate to some extent. The beams in group SP3 are in a state of axial compression, and the compressive stress is uniformly distributed along the section height. By comparison, the beams in group SP5 are in a state of eccentric compression, and the compressive stress is in a linear distribution along the section height. However, comparing the carbonation depths of specimens SP3-1-40 (3.6 mm), SP5-3-40 (3.8 mm), and SP3-1-50 (2.7 mm), SP5-3-50 (2.8 mm), respectively, which have the same compressive stress of $0.3f_c$ at beam bottom on the 28^{th} day of carbonation. It is found that the carbonation depth values are almost the same under the same concrete strength.

In fact, as concrete carbonation is developed in the superficial layer of the specimen where the stress values are basically the same, it is acceptable for some scholars to equate the carbonation depths of concrete under axial compression to those under eccentric compression [32].

3.4. Influence of Concrete Strength (Water-Cement Ratio). According to the research [11–14], different concrete strengths (water-cement ratios) will have marked impacts on the carbonation rate for concrete. The smaller the concrete strength in a certain range, the faster the carbonation rate. These scholars take the concrete strength as the main independent variable to give their own carbonation prediction formulas.

The experimental results in this paper have verified the corrosion laws of the pieces of research. In all these five testing groups, the carbonation rates of specimens with different concrete strengths are obviously different. For example, it can be seen from Figure 6(d) that the carbonation depths of specimens of C40 concrete are much higher than those of C50 concrete under different compressive stress levels after 28 days of carbonation corrosion, and the average difference in carbonation depth is about 0.85 mm.

3.5. Coupling Effects of Chloride Corrosion, Concrete Strength, and Stress State. As shown in Figure 6(a), compared with the carbonation depths of specimens in group SP1, the carbonation depths of specimens in group SP2 with different concrete strengths still have a clear distinction. An evident conclusion is drawn that the concrete strength will have a significant impact on the carbonation rate whether under the chloride corrosion or not. However, with the increase of concrete strength, the sensitivity of its effect on the carbonation rate is reduced. It can be easily verified from the test data of carbonation depths in Figure 6(a). To better reflect the coupling effect of chloride corrosion and water-cement ratio on carbonation rate, the depth differences of carbonation between the specimens of C40 and C50 concrete are calculated, respectively. Specifically, after continuous carbonation for 28 days, the carbonation depth of SP1-40 is 36.6 percent higher than that of SP1-50, while the carbonation depth of SP2-40 is 25 percent higher than that of SP2-50. In the experiment, the combined effects of chloride corrosion and concrete strength reduce the carbonization depth of specimens of C50 concrete by 16.2 percent on average when compared with those of C40 concrete.

To further analyze the coupling effects of chloride erosion, water-cement ratio, and stress state on carbonation rate, the carbonation depths of partial specimens after carbonizing for 28 days and their depth differences (Δd) are calculated and listed in Table 3. It can be seen vividly that compared with other specimens, the carbonation depths of SP1-40/50 are much deeper with great Δd between them. It, once again, shows that chloride corrosion has a strong inhibition effect on carbonation. Besides, with the decrease of the tensile stress level or the increase of the compressive stress level, the carbonation depths show a clear downward trend, however, the Δd between them with different concrete grades still keeps great values. Therefore, the influence of the change of concrete strength is greater when the stress level is higher.

Table 3: Carbonation depths of partial specimens after carbonizing for 28 days under different corrosion conditions.

Specimen number	Stress at beam bottom (MPa)	d_1 (mm)	d_2 (mm)	$\Delta d = d_2 - d_1$ (mm)	$\delta = \Delta d/d_1$ (%)
SP1-40/50	—	11.2	8.2	−3.0	−26.8
SP4-3-40/50	$0.5f_t$	4.7	3.9	−0.8	−17.0
SP4-2-40/50	$0.3f_t$	4.6	3.8	−0.8	−17.4
SP2-40/50	0	4.5	3.6	−0.9	−20.0
SP5-2-40/50	$0.15f_c$	3.9	3	−0.9	−23.0
SP3-1-40/50	$0.3f_c$	3.8	2.9	−0.9	−23.7
SP3-2-40/50	$0.5f_c$	3.5	2.6	−0.9	−25.7
SP3-3-40/50	$0.7f_c$	3.3	2.4	−0.9	−27.3

Note. d_1 and d_2 are the carbonation depths of the specimens with concrete grades of C40 and C50, respectively.

4. Mechanical Investigation

4.1. Evaluation of the Corrosion Degree of Steel Rebars. It is well-known that the corrosion of steel in the reinforced concrete structure would directly affect the mechanical property of concrete. Hence, its corrosion rate should be measured to evaluate the corrosion degree of steel. For specimens in groups SP4 and SP5, stirrups and longitudinal reinforcements with a length of about 50 cm were cut out and cleaned using dilute hydrochloric acid at room temperature, and if necessary, manual cleaning using a wire brush is efficient to remove the rust on the steel surface. The cleaning time was controlled within 1~5 minutes. After the cleaning, the alkaline water was used to neutralize residual dilute hydrochloric acid on the steel surface, and then the well-treated steel rebars were stored in the desiccator for 4 hours.

After the steel rebars were completely dry, an electronic balance with a measuring accuracy of 0.01 g and a steel tape with a measuring precision of 0.5 mm were adopted to measure the weight (m) and the length (l) of the steel rebars, respectively. The average linear density (ρ) of the steel rebar can be calculated as follows:

$$p = \frac{m}{l}. \tag{1}$$

Here in this paper, the average section corrosion rate (η) is used to describe the corrosion degree of the steel bars, which can be described as follows:

$$\eta = \frac{\rho_0 - \rho_c}{\rho_0} \times 100\%, \tag{2}$$

in which ρ_0 and ρ_c are the average linear densities of noncorroded steel rebars before the corrosion test and corroded steel rebars after the corrosion test, respectively.

The specific values η of specimens in groups SP4 and SP5 are listed in Tables 4 and 5 below. It is found that the corrosion degree of steel rebars would decrease with the increase of concrete strength. Also, with the decrease of tensile stress or the increase of the compressive stress level, the corrosion rate of steel rebars would be inhibited obviously.

4.2. Failure Modes. For long beam specimens in group SP4, the bending test was conducted after the corrosion test. The failure process of the specimens was observed from zero loads up to ultimate loads. At first, with small load values, the beam can keep good work performance. Then, cracks began to appear at the bottom of the beam with the increase of load. The concrete in the tension area will not bear load anymore after cracking, however, the stress of the steel bars in the tension area will continue to increase until the yield strength. After this stage, the steel bars generated great plastic deformation, and the concrete crack developed rapidly. The deflection of the beam also increased sharply. When the maximum strain on the compressive concrete reached its limited value, the concrete in the compression zone was crushed and the beam was finally destroyed, as shown in Figure 7.

Similar to the failure mode of ordinary reinforced concrete long beams, the failure of these beams belongs to the bending plastic failure with steel yield-concrete crushing. Because of the small corrosion degree of steel rebars, the tension reinforcement in concrete could not be snapped during the whole loading process.

For short beam specimens in group SP5, the shear test was conducted after the corrosion test. The failure pattern of these beams is shear-compress.

When loads were small, the diagonal flexure-shear cracks were gradually produced in the shear-bending zone of the beam. With the increment of the loading values, one main diagonal crack with longer extension and wider-ranging distribution would occur and then extend to the loading location. Finally, the concrete in the shear-compression zone was broken under the combined action of the shear stress and normal stress, as shown in Figure 8. In addition, the beams could also be damaged by the development of the corrosive cracks caused by the corrosion and expansion pressure of stirrups. As the corrosion degree of stirrups was small with relatively high elongation and good ductility, the stirrups were found not to be broken throughout the loaded process.

4.3. Developing Feature of Concrete Cracks. For specimen SP4-0-40 with no corrosion, cracks began to appear in the pure bending section of beams when the applied load level was equal to or exceeded about 15% of the ultimate load (F_u), and for SP4-0-50, this load level was about $0.18F_u$. When the load level increased to $0.43F_u$ for SP4-0-40 or $0.63F_u$ for SP4-0-50, several cracks extended to the centroidal axis position of the beam. The maximum crack width of beams was about 0.2 mm at load $0.8F_u$. Finally, it could find about 6 cracks in

Table 4: Ultimate load of flexural beams.

NO.		η (%)	F_{max} (kN)	ω_{max} (mm)	M_{uc} or M_{u0} (kN·m)	M_r (%)	κ_b	d	d_{r1}	d_{r2} (%)
SP4-0-40	CI-0	0	18.60	29.92	7.44	—	1	7.37	1	—
SP4-1-40	CI-1	2.7	18.02	29.15	7.21	−3.1	0.969	7.22	0.979	−2.0
SP4-2-40	CI-2	5.1	17.31	29.01	6.92	−7.0	0.931	6.94	0.942	−5.8
SP4-3-40	CI-3	7.3	17.10	29.68	6.84	−8.1	0.919	6.60	0.895	−10.4
SP4-0-50	CII-0	0	22.28	37.20	8.91	–	1	9.92	1	–
SP4-1-50	CII-1	1.8	21.81	34.87	8.72	−2.1	0.979	9.25	0.932	−6.8
SP4-2-50	CII-2	2.6	21.56	34.01	8.62	−3.3	0.968	8.25	0.831	−16.8
SP4-3-50	CII-3	3.9	21.29	37.12	8.52	−4.4	0.956	8.71	0.878	−12.2

Note. M_{uc} and M_{u0} is the ultimate bending moment of the corroded flexural beam and the noncorroded flexural beam, respectively, and $\kappa_b = M_{uc}/M_{u0}$. F_{max} denotes the ultimate load. ω_{max} denotes ultimate deflection. d denotes ductility, $d = f_u/f_y$, f_u is the ultimate displacement, f_y is the yield displacement. d_{r1} denotes the ductility ratio of corroded beams to noncorroded beams. d_{r2} denotes the ductility change rate of the corroded beam relative to the noncorroded beam. M_r denotes the ultimate bending moment change rate of the corroded beam relative to the noncorroded beam.

Table 5: Ultimate load of shearing beams.

NO.		η (%)	V_{uc} or V_{u0} (kN)	F_r (%)	ω_{max} (mm)	κ_s	d	d_r	d_{r2} (%)
SP5-0-40	DI-0	0	46.19	—	12.07	1	5.09	1.000	—
SP5-1-40	DI-1	1.7	45.28	−2.0	5.14	0.980	3.25	0.639	−36.1
SP5-2-40	DI-2	3.2	43.76	−5.3	7.24	0.947	4.67	0.917	−8.3
SP5-3-40	DI-3	4.4	42.32	−8.4	7.08	0.916	4.51	0.885	−11.4
SP5-0-50	DII-0	0	51.79	—	9.72	1	6.57	1.000	—
SP5-1-50	DII-1	1.5	49.44	−4.5	8.56	0.955	4.73	0.720	−28.0
SP5-2-50	DII-2	2.8	48.87	−5.6	7.44	0.944	4.56	0.695	−30.6
SP5-3-50	DII-3	4.0	45.95	−11.3	7.34	0.887	4.77	0.726	−27.4

Note. V_{uc} and V_{u0} are the ultimate shear loads of the corroded beam and the noncorroded beam, respectively, and $\kappa_s = V_{uc}/V_{u0}$. F_r denotes the ultimate load change rate of the corroded beam relative to the noncorroded beam.

(a) (b)

Figure 7: The failure modes of specimens in group SP4. (a) Specimen SP4-0-50 without corrosion. (b) Specimen SP4-3-50.

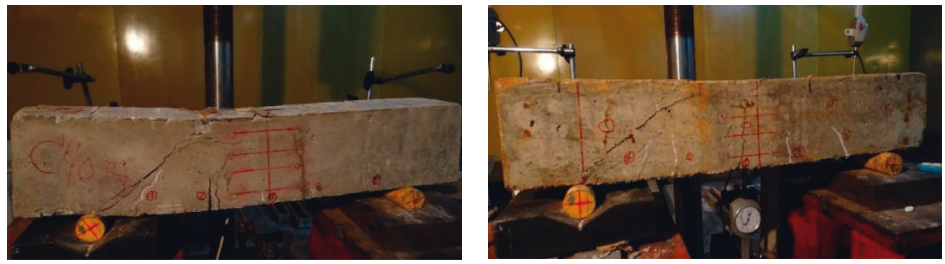

(a) (b)

Figure 8: The failure modes of specimens in group SP5. (a) Specimen SP5-0-40 without corrosion. (b) Specimen SP5-3-50.

SP4-0-40 and 4 cracks in SP4-0-50, and their crack widths were wider than 1 mm at the ultimate load.

For corroded reinforced concrete specimens in group SP4 with the capability deteriorating of the internal bond between the steel bar and concrete considered, the number of cracks was decreased and the distances between the two cracks were increased compared with specimens with no corrosion. According to the test results, the number of

cracks in the corroded beams was generally 3~7 with an uneven crack distribution. When the load level reached $0.8F_u$, one crack in the pure bending section would develop rapidly, while other cracks developed slowly. Besides, as the steel corrosion rate increases, the number of cracks tends to decrease, and the crack distribution tends to converge toward the middle span.

Generally, because of the combined corrosion action of chloride ions and CO_2, the bonding performance between the steel rebars and concrete would degenerate obviously. Therefore, steel rebars would not be able to work collaboratively with concrete, causing the deterioration of the uniformity of crack distribution.

For noncorrosion beams, the crack distribution was uniform, and the number of cracks was 5~7. Cracks gradually developed from the bottom of the beam, and the diagonal shear cracks were extended from the support to the loading point, with the load increasing. It was measured that the maximum crack width was about 1.5 mm at the peak load.

Similar to the developing feature of cracks in group SP4, the crack distribution was also not uniform and irregular for corroded beams in group SP5. During the loading process, the crack development was mostly dominated by one main crack. Also, the cracking directions were easily affected and changed by the rust expansion crack, especially for diagonal shear cracks, and accompanied by partial concrete spalling in the shear zone of the beam. Statistics showed that the number of cracks in these beams was within the range of 3 to 5, and the maximum crack width was about 1.2 mm at the ultimate load.

4.4. Characteristics of Strain and Deflection. During the loading test, the strain and deflection data at the midspan were measured. When the applied load is 10 kN, the strain distribution of data at a different height of each beam at the midspan section is shown in Figure 9. Also, the strain distribution of the same beam under different loads can be obtained. Figure 10 shows the strain distribution by different loads at the midspan section of the corroded beams CI-2 and CII-2. Upon comparing these test results, it is found that the concrete strain of the corroded beam is larger than that of the noncorroded beam under the same load by and large, and the height of the compression zone of the corroded beam is smaller than that of the noncorroded beam. In addition, we can see from Figure 10 that the concrete strain at the midspan section of the concrete beam still conforms to the plane section assumption macroscopically. This conclusion is consistent with the data in literature [28, 31].

According to the load-deflection curves of the long beams, shown in Figures 11(a) and 11(b). It can be seen that before the load reaches about 60% of the ultimate load of the beam, the load-deflection curves of the corroded beam and the noncorroded beam basically coincide with each other. When the load further increases, the difference between the corroded beam and the noncorroded beam is gradually significant. Under the same load, the deflection of test beams increases with the increase of the section corrosion rate of reinforcement.

Figures 11(a) and 11(b) also illustrate that the deformation capacity of corroded beams is significantly lower than that of the noncorroded beams. The ductility ratio of corroded beams to noncorroded beams is 0.831~0.979. The ductility of corroded beams decreases by 2.0%~16.8% compared with that of noncorroded beams, and the larger the corrosion rate, the more the ductility reduction, as shown in Table 4.

The strain distribution at the midspan of each beam under the load of 25 kN is shown in Figure 12. The strain distribution of DI-2 beam and DII-2 beam in the midspan under different loads is shown in Figure 13. The characteristics of the load-deflection curves of beams in shearing experiments are similar to those in bending experiments, except that the maximum vertical displacement ω_{max} is much smaller, as shown in Figures 11(c) and 11(d). For DI group, with the increase in corrosion rate from 1.7%, 3.2%, and 4.4%, the ultimate deflection decreases by 57.4%, 40%, and 41.3%, respectively, and the ductility ratio decreases by 36.1%, 8.3%, and 11.5%, respectively. For DII group, with the increase in corrosion rate from 1.5%, 2.8%, and 4.9%, the ultimate deflection decreases by 11.9%, 23.5%, and 24.5% compared with that of a noncorroded beam, and its ductility ratio decreases by 28.0%, 30.5%, and 27.4%, respectively, as shown in Table 5.

4.5. Analysis of Bearing Capacity. The deflection of corroded beams increases with the increase of the corrosion rate of reinforcement. That is to say, the rigidity of the test beam decreases with the increase of the corrosion rate, which, as a result, leads to the decline of flexural capacity. The ultimate load of each test beam is given in Table 4.

For group CI, it can be seen from Table 4 that with the increase in corrosion rate from 2.7%, 5.1%, and 7.3%, the ultimate load of the corroded long beams of the CI group reduces by 3.1%, 6.9%, and 8.1%, respectively. The ultimate bending moment is 3.1%, 6.9%, and 8.1% lower than that of the beam without corrosion.

For group CII, with the increase of the corrosion rate from 1.8%, 2.6%, and 3.9%, the ultimate load of the corroded beams decreases by 2.1%, 3.2%, and 4.4%, respectively, and the ultimate bending moment decreased by 2.1%, 3.2%, and 4.4%, respectively.

The above results show that the ultimate load, deflection, and bending moment of the two groups of beams decrease with the increase of the degree of corrosion, and they show a significant correlation with the corrosion rate [30, 31]. Therefore, we try to find the relationship between the corrosion rate of reinforcement and the ultimate bearing capacity.

The relative ultimate flexural strength κ_b is defined as the ratio of the ultimate bending moment M_{uc} of the corroded flexural beam and the ultimate bending moment M_{u0} of the noncorroded flexural beam. It is a dimensionless parameter to describe the change of the ultimate strength of the corroded flexural beam, which is calculated as follows:

$$M_{uc} = k_b M_{u0}. \tag{3}$$

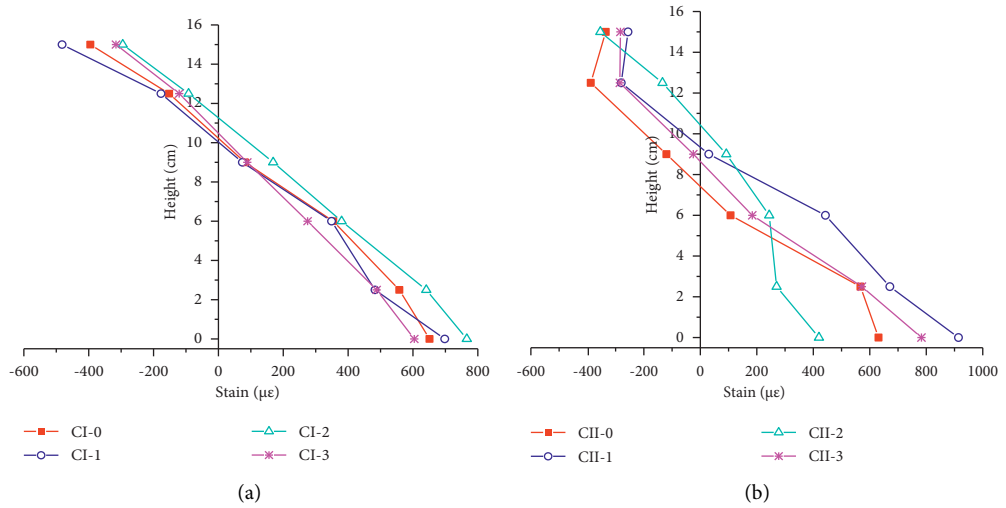

Figure 9: Section strain distribution of different beams under the load of 10 kN. (a) CI and (b) CII.

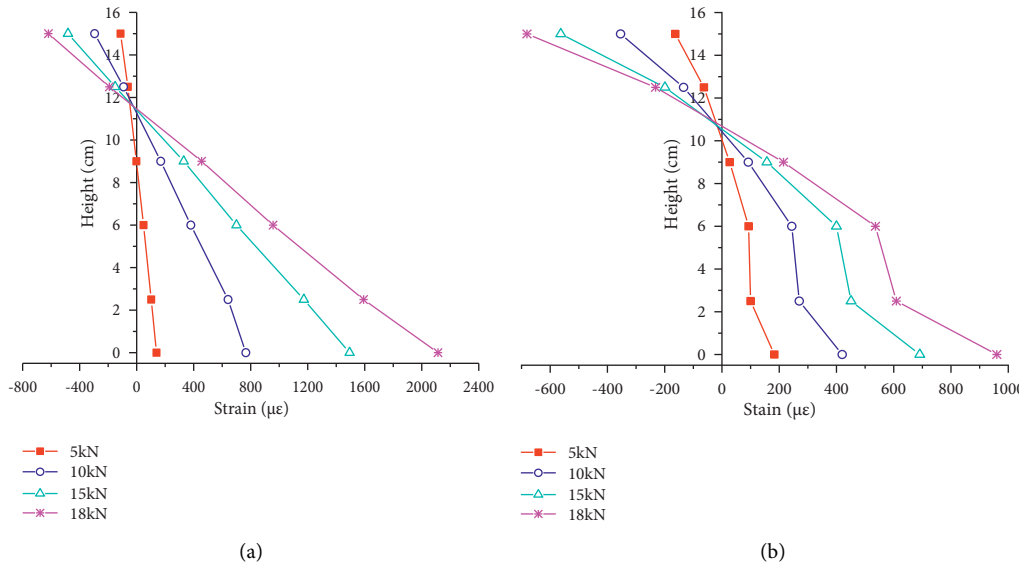

Figure 10: Section strain distribution by different loads in bending tests. (a) CI and (b) CII.

The parameter κ_b of each test beam is shown in Table 4. Through regression analysis of the data, the κ_b–η curve can be obtained as shown in Figure 14(a), which shows a good linear relationship. Therefore, we get the formula for calculating the flexural capacity of the corroded reinforced concrete beams as follows: $\kappa_b = 1–1.1802\eta$, correlation coefficient $R = –0.99085$, and $R^2 = 0.9818$.

Table 5 shows that with the increase in corrosion rate from 1.7%, 3.2%, and 4.4%, the ultimate load of group DI (corroded short beams) decreased by 2.0%, 5.3%, and 8.4% compared with that of a noncorroded beam. With the increase in corrosion rate from 1.5%, 2.8%, and 4.9%, the ultimate load of group DII short beam decreased by 4.5%, 5.6%, and 11.3% compared with that of a noncorroded beam. The ultimate load of the corroded beams decreases with the increase in corrosion rate.

Similar to the flexural capacity, the relative ultimate shear strength κ_s is defined as the ratio of the ultimate shear load V_{uc} of the corroded beam to the ultimate shear load V_{u0} of a noncorroded beam. There is a good linear relationship between κ_s and η, as shown in Figure 14(b). $\kappa_s = 1–2.0718\eta$, correlation coefficient $R = –0.9643$, and $R^2 = 0.9182$.

Evidently, the slope of the curve κ_s–η is much larger than that of the curve κ_b–η, which indicates that the influence of the stirrup corrosion rate on shear capacity is much greater than that on bending capacity. It is because the shear strength of ordinary concrete is much lower than its compressive strength, and the shear capacity of RC beams is mostly provided by stirrups.

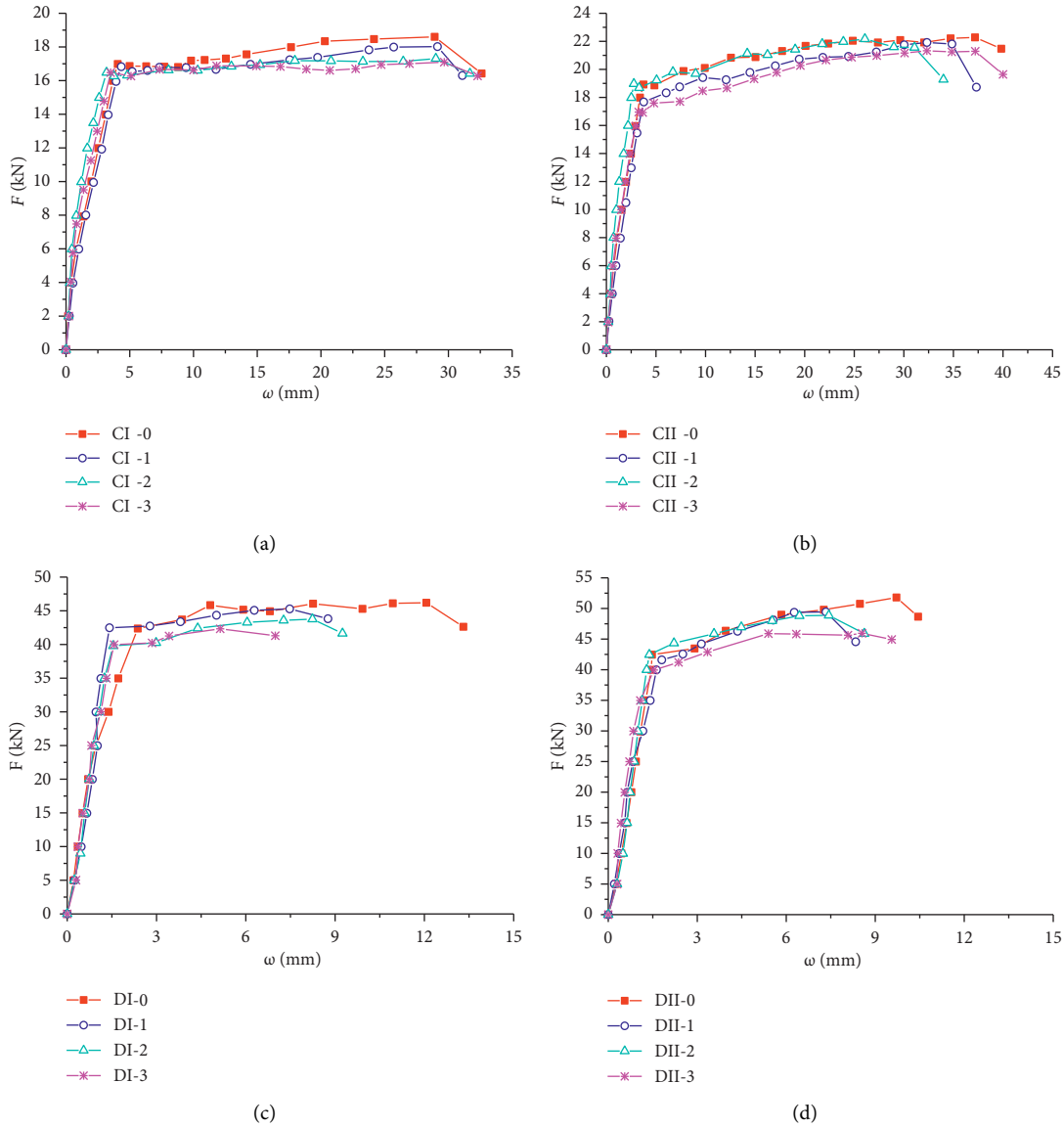

Figure 11: Load-deflection curve of test beams. (a) CI, (b) CII, (c) DI, and (d) DII.

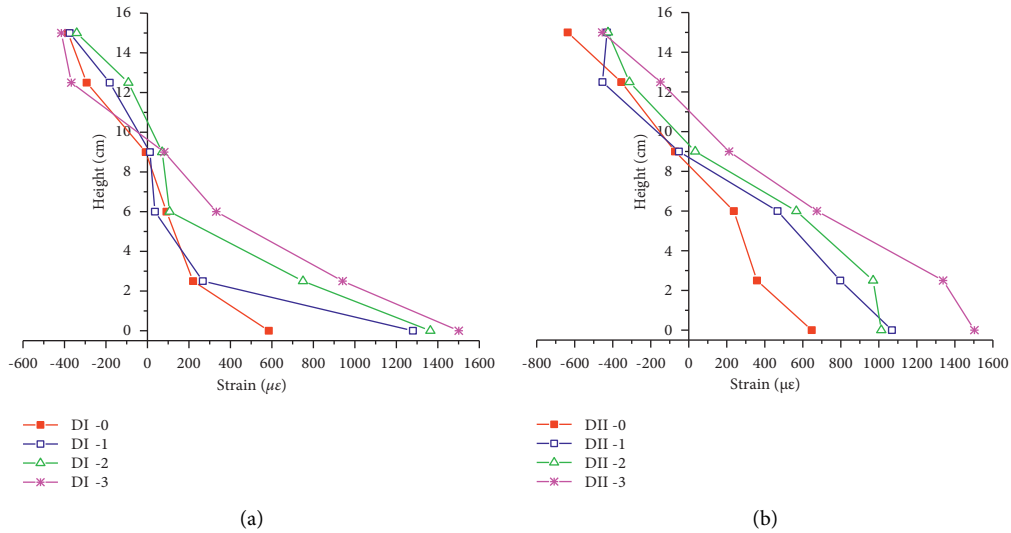

Figure 12: Section strain distribution of different beams under the load of 25 kN. (a) DI and (b) DII.

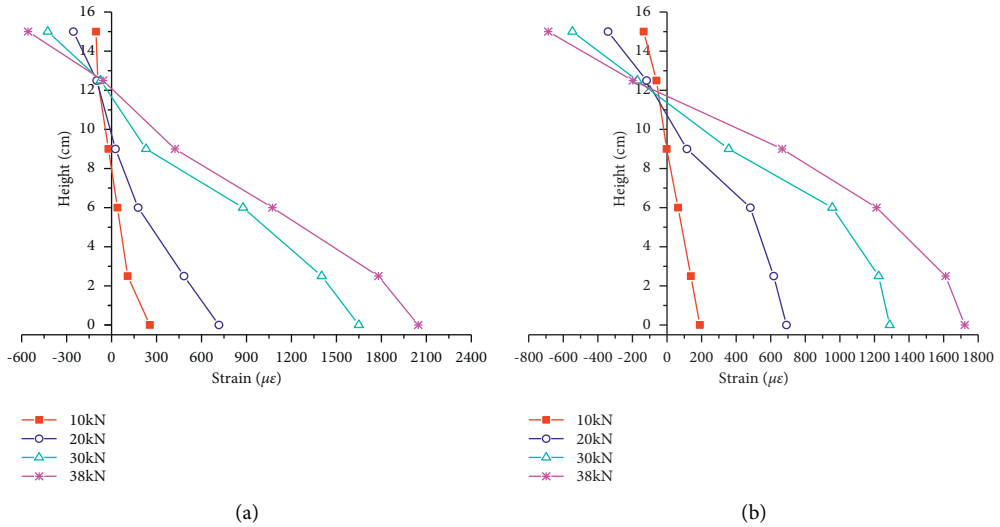

Figure 13: Section strain distribution by different loads in shearing tests. (a) DI and (b) DII.

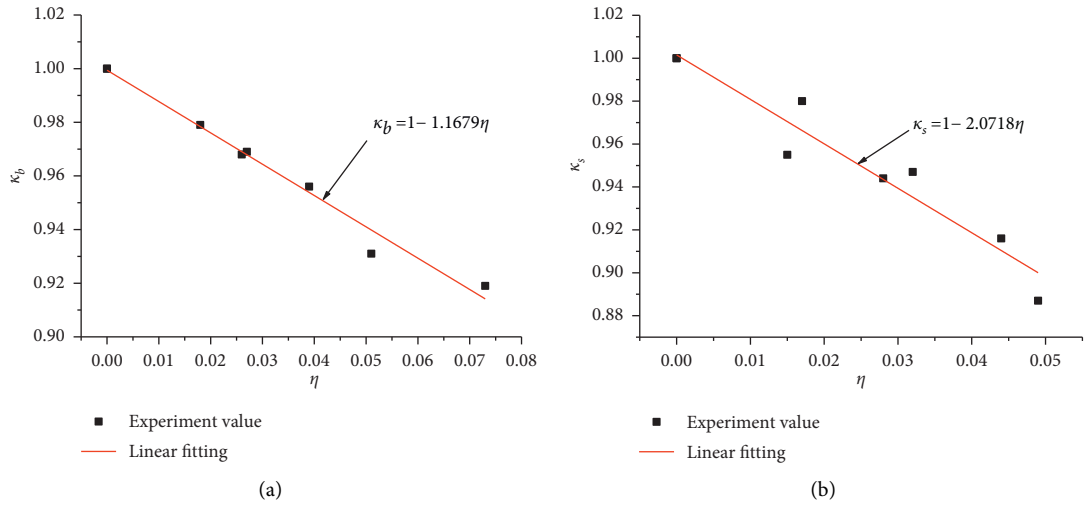

Figure 14: Relationship between relative ultimate strength and corrosion rate. (a) κ_b–η and (b) κ_s–η.

5. Conclusions

In this study, the carbonation characteristics of RC beams under the coupled effects of chloride erosion and different stress states were discussed by experiment, and the attenuation law and failure modes of the flexural and shearing capacity of the corroded RC beams under these coupled corrosion factors were investigated. The drawn conclusions are summarized as follows:

(1) Chloride corrosion can reduce the carbonation rate by 56% ~ 60%. A different strength or water-cement ratio has a significant impact on the carbonation rate, however, when chloride corrosion and carbonation are coupled, the impact is significantly reduced.

(2) The applied tensile stress promotes carbonation and chloride erosion and aggravates the corrosion of steel bars, however, the effect of compressive stress is the opposite. It is feasible to study the carbonation of a concrete bridge by replacing the prestressed compressive stress with axial compressive stress.

(3) With the increase in steel corrosion rate, the number of cracks in corroded RC beams tends to decrease compared with that in noncorroded beams, and the distribution of cracks tends to be close to the midspan. Under the same load, the concrete strain of the corroded beam is larger than that of the noncorroded beam, and the height of the compression zone of the corroded beam is smaller than that of the noncorroded beam.

(4) Under a low corrosion rate (<10%), the failure mode of a flexural beam is a concrete-crushing failure in the compression area, and the failure mode of a shear beam is a concrete-crushing failure in the shear-compression surface. With the increase in the corrosion degree of the bars, the bending and shear capacity of the corroded beam gradually decreases,

and the stiffness and deformation capacity are gradually weakened.

(5) The relationship between the relative ultimate shear strength of the beam and the average corrosion rate of the stirrup section is approximately linear. The relationship between the relative ultimate flexural strength of the beam and the average corrosion rate of the longitudinal reinforcement section is approximately linear.

Data Availability

The data used to support the findings of this study are available from the corresponding author upon request.

Conflicts of Interest

The authors declare that there are no conflicts of interest regarding the publication of this paper.

References

[1] V. G. Papadakis, C. G. Vayenas, and M. N. Fardis, "A reaction engineering approach to the problem of concrete carbonation," *AIChE Journal*, vol. 35, no. 10, pp. 1639–1650, 1989.

[2] S. A. Meier, M. A. Peter, A. Muntean, and M. Böhm, "Dynamics of the internal reaction layer arising during carbonation of concrete," *Chemical Engineering Science*, vol. 62, no. 4, pp. 1125–1137, 2007.

[3] A. B. Muntean, M. Kropp, and J. Kropp, "Moving carbonation fronts in concrete: a moving-sharp-interface approach," *Chemical Engineering Science*, vol. 66, no. 3, pp. 538–547, 2011.

[4] https://research.noaa.gov/article/ArtMID/587/2636/Rise-of-carbon-dioxide-unabated.

[5] I. S. Yoon, O. Çopuroğlu, and K. B. Park, "Effect of global climatic change on carbonation progress of concrete," *Atmospheric Environment*, vol. 41, no. 34, pp. 7274–7285, 2007.

[6] V. G. Papadakis, C. G. Vayenas, and M. N. Fardis, "Fundamental modeling and experimental investigation of concrete carbonation," *ACI Materials Journal*, vol. 88, no. 4, pp. 363–373, 1991.

[7] V. G. Papadakis, "Physical and chemical characteristics affecting the durability of concrete," *Aci Material Journal*, vol. 8, no. 2, pp. 186–196, 1991.

[8] V. G. Papadakis, C. G. Vayenas, and M. N. Fardis, "Experimental investigation and mathematical modeling of the concrete carbonation problem," *Chemical Engineering Science*, vol. 46, no. 5/6, pp. 1333–1338, 1991.

[9] V. G. Papadakis, "Effect of supplementary cementing materials on concrete resistance against carbonation and chloride ingress," *Cement and Concrete Research*, vol. 67, no. 30, pp. 291–299, 2000.

[10] L. Czarnecki and P. Woyciechowski, "Modelling of concrete carbonation; is it a process unlimited in time and restricted in space?" *Bulletin of the Polish Academy of Sciences, Technical Sciences*, vol. 63, no. 1, pp. 43–54, 2015.

[11] A. G. Magalhães, F. J. Silva, M. A. P. Rezende, W. J. Santos, E. V. M. Carrasco, and J. N. R. Mantilla, "The influence of the water/cement ratio in the open porosity and in the carbonation front advancing in cementitious matrix composites," *Applied Mechanics and Materials*, vol. 864, pp. 313–317, 2017.

[12] L. Xu and S. Huang, "The mathematical model of predicted carbonation depth in concrete," *Journal of Building Materials*, vol. 6, no. 4, pp. 347–357, 1991, (in Chinese).

[13] A. D. M. Arachchige, "Influence of cement content on corrosion resistance," *Proceedings of the Institution of Civil Engineers - Construction Materials*, vol. 161, no. 1, pp. 31–39, 2008.

[14] N. R. Buenfeld and E. Okundi, "Effect of cement content on transport in concrete," *Magazine of Concrete Research*, vol. 50, no. 4, pp. 339–351, 1998.

[15] D. Niu, Y. Chen, and S. Yu, "Model and reliability analysis for carbonation of concrete structures," *Journal of Xi'an University of Architecture and Technology*, vol. 22, no. 4, pp. 365–369, 1995.

[16] Y. Wang, X. Jiang, S. Wang et al., "Influence of axial loads on CO2 and Cl− transport in concrete phases: paste, mortar and ITZ," *Construction and Building Materials*, vol. 204, no. APR.20, pp. 875–883, 2019.

[17] C. Jiang, X. Gu, W. Zhang, and W. Zou, "Modeling of carbonation in tensile zone of plain concrete beams damaged by cyclic loading," *Construction and Building Materials*, vol. 77, no. feb.15, pp. 479–488, 2015.

[18] Z. H. O. N. G. Xiao-ping, C. A. O. Da-fu, and P. Huang, "Model study of practical random probability of concrete carbonation under influences of various factors," *World Bridges*, vol. 36, no. 3, pp. 32–34, 2006.

[19] P. Akpinar and I. D. Uwanuakwa, "Investigation of the parameters influencing progress of concrete carbonation depth by using artificial neural networks," *Materiales de Construcción*, vol. 70, no. 337, 2020.

[20] S. J. Kwon and H. W. Song, "Analysis of carbonation behavior in concrete using neural network algorithm and carbonation modeling," *Cement and Concrete Research*, vol. 40, no. 1, pp. 119–127, 2010.

[21] J. Sun and L. Lu, "Coupled effect of axially distributed load and carbonization on permeability of concrete," *Construction and Building Materials*, vol. 79, no. mar.15, pp. 9–13, 2015.

[22] H. Ye, X. Jin, C. Fu, N. Jin, Y. Xu, and T. Huang, "Chloride penetration in concrete exposed to cyclic drying-wetting and carbonation," *Construction and Building Materials*, vol. 112, no. jun.1, pp. 457–463, 2016.

[23] X.-H. Wang, D. V. Val, and Li. Zheng, "Carbonation of loaded RC elements made of different concrete types: accelerated testing and future predictions," *Construction and Building Materials*, vol. 64, 2020.

[24] Y. Y. Miao, D. T. Niu, and N. Cheng, "Durability of concrete under the combined action of carbonization and fatigue loading of vehicles," *Science of Advanced Materials*, vol. 25, 2019.

[25] P. Konecny, P. Lehner, and D. Vorechovska, *Evaluation of durability-related field inspection data from concrete bridges under service*, vol. 65, no. 1, pp. 81–89, 2020.

[26] M. J. Osmolska, T. Kanstad, M. A. N. Hendriks, K. Hornbostel, and G. Markeset, "Durability of pretensioned concrete girders in coastal climate bridges: basis for better maintenance and future design," *Structural Concrete*, vol. 20, no. 6, pp. 2256–2271, 2019.

[27] Y. Tian, J. Liu, H. Xiao et al., "Experimental study on bond performance and damage detection of corroded reinforced concrete specimens," *Advances in Civil Engineering*, vol. 12, 2020.

[28] A. Torres-Acosta, S. Navarro-Gutierrez, and J. Terán-Guillén, "Residual flexure capacity of corroded reinforced concrete

beams," *Engineering Structures*, vol. 29, no. 6, pp. 1145–1152, 2007.

[29] D. V. Val and L. Chernin, "Serviceability reliability of reinforced concrete beams with corroded reinforcement," *Journal of Structural Engineering*, vol. 135, no. 8, pp. 896–905, 2009.

[30] G. Campione, F. Cannella, and L. Cavaleri, "Shear and flexural strength prediction of corroded R.C. beams," *Construction and Building Materials*, vol. 149, no. 15, pp. 395–405, 2017.

[31] G. Campione and F. Cannella, "Engineering failure analysis of corroded R.C. beams in flexure and shear," *Engineering Failure Analysis*, vol. 86, pp. 100–114, 2018.

[32] Y. Tu and L. ü Zhitao, "Research on the experiment of prestressed concrete structures in carbonation environment and the prediction model of carbonation depth," *Industrial Construction*, vol. 36, no. 1, pp. 47–50, 2006.

[33] W. Puatatsananon and V. E. Saouma, "Nonlinear coupling of carbonation and chloride diffusion in concrete," *Journal of Materials in Civil Engineering*, vol. 17, no. 3, pp. 264–275, 2005.